A Stabilized Eighteen-Node Solid Element for Hyperelastic Analysis of Shells

K.Y.Sze[#] , **S.-J.Zheng**[#]* and **S.H.Lo**[$]

[#]*Department of Mechanical Engineering,* [$]*Department of Civil Engineering,*

The University of Hong Kong, Pokfulam Road, Hong Kong SAR, P.R.CHINA

SUMMARY

The objective of the present study is to develop a solid element for large deformation analysis of hyperelastic shell structures. To attain high computational efficiency and annihilate shear and membrane lockings, a hybrid-strain stabilization approach is adopted. To overcome the thickness locking of the element, the enhanced assumed thickness strain modes are incorporated. Starting from the virtual work principle and a weak form that enforces the equality of the hybrid-strain and the strain arising from the displacement and the enhanced assumed strain, an eighteen-node element for large deformation analysis of hyperelastic shells is developed. The salient feature of the present element for higher computational efficiency is that the element uses only the second order quadrature for integration along the two in-plane natural coordinates and the stabilization vectors can be formed without using any integration loops. Efficacy of the element is illustrated by popular benchmark problems.

* Present address : *Nanjing University of Aeronautics & Astronautics, Nanjing 210016, P.R.CHINA*

Keywords : solid-shell, hybrid-strain, hyperelasticity, enhanced assumed strain, stabilization.

Published in Finite Elements in Analysis and Design 40 (2004) 319–340

1. INTRODUCTION

Rubber components are employed in various branches of modern engineering constructions. To develop reliable and accurate numerical analysis models, the following noteworthy difficulties should be considered carefully including element robustness and efficiency, incompressibility and large deformation hyperelasticity. The challenge in the simulation of hyperelastic materials in large deformation analysis of shell structures is met with much attention, and a great deal of publications could be cited [1-17]. Many constitutive models have been proposed in the literatures for the numerical simulation of hyperelastic materials. A formulation widely used for this purpose is the Mooney–Rivlin model including as a special case the Neo-Hookean material, where the strain energy function is expressed in terms of the invariants of the right Cauchy-Green tensor [1,4,7-11,13-16]. Another possibility is the use of Ogden model, with a strain energy density formulated in terms of the principal stretches [2,3,5,6,12], which is however one of the most complicated constitutive laws employed in numerical realization as it requires the transformation between tensor components related to principal axes and components related to different coordinate axes.

The main incentive of the present contribution comes from the observation that the finite element formulation for hyperelastic materials has not been satisfactory, especially for the large deformation analysis of shell structures. Much of the efforts have been focused on the simulation of plane problems [6,8,9,11], membrane shells [2,3] and axisymmetric shell models [5], and only in recent years, the hyperelastic models for shell analysis have attracted the attention of several investigators [12-17]. Hyperelastic shells are very flexible structures able to undergo both finite rotation and large strain. In geometrical sense, large strain phenomena are characterized by significant thickness changes and may also involve finite rotations. The current available shell elements are mainly developed within the context of the so-called degenerated approach, where common assumptions are inextensible director and the zero thickness stress condition. However, the large strain constitutive algorithms under the plane-stress constraint can be very cumbersome and also may not be an appropriate assumption fully justified for general large deformation problems [16]. Consequently, some researchers [15-17] adopted directly the general three-dimensional constitutive law without modification. The practice necessitates the so-called solid-shell elements which can tackle shell analyses without exhibiting various locking deficiencies .

Without any rotational d.o.f.s, solid-shell elements are particularly convenient for geometrical nonlinear analyses [16-22]. Some researchers extended them to the large strain analysis of hyperelastic materials, employing mostly lower order elements [15,17]. Recently, the first author and his colleagues have presented promising lower and higher order hybrid-stress solid-shell elements for linear and geometric nonlinear analyses of homogeneous and laminated shells [20-26].

Nevertheless, these hybrid-stress elements cannot be readily extended to hyperelastic material analysis as the constitutive law of the materials are always expressed in terms of the strain energy potentials which are functions of the strain. In this paper, a hybrid-strain element is developed for large deformation analysis of hyperelastic shells. Unlike the previous elements which are all eight-node in configuration [15,17], the present element is an eighteen-node one. To avoid various locking phenomena, a stabilization approach and four enhanced assumed strain (EAS) modes for the natural thickness strain component are incorporated [1,15]. The hybrid-strain field is selected in a way similar to that of a previously developed geometric nonlinear eighteen-node element for linear homogeneous and laminated materials. Upon simplifications, the nonlinear element equation turns out to be just slightly more complicated than that of the Uniform Reduced Integrated (URI) element. Efficacy of the element is illustrated by a number of commonly employed benchmark problems.

2. DISPLACEMENT-DERIVED AND ENHANCED ASSUMED STRAINS

Figure 1 shows the eighteen-node element under consideration. The initial or undeformed coordinate vector **X** and the displacement vector **U** are interpolation in the standard manner,

$$\mathbf{X}(\xi,\eta,\zeta)=\sum_{j=1}^{9}N_j(\xi,\eta)(\zeta^{+}\mathbf{X}_j+\zeta^{-}\mathbf{X}_{9+j})=\mathbf{X}_o(\xi,\eta)+\zeta\mathbf{X}_n(\xi,\eta)=\mathbb{N}_o(\xi,\eta)\underline{\mathbf{X}}+\zeta\mathbb{N}_n(\xi,\eta)\underline{\mathbf{X}},$$
$$\mathbf{U}(\xi,\eta,\zeta)=\sum_{j=1}^{9}N_j(\xi,\eta)(\zeta^{+}\mathbf{U}_j+\zeta^{-}\mathbf{U}_{9+j})=\mathbb{N}_o(\xi,\eta)\underline{\mathbf{U}}+\zeta\mathbb{N}_n(\xi,\eta)\underline{\mathbf{U}} \qquad (1)$$

where (ξ,η,ζ) are the natural or isoparametric coordinates, $\mathbf{X}_j$ is the nodal counterpart of **X** and $\mathbf{U}_j$ is the nodal counterpart of **U**. Moreover,

$$\zeta^{+}=\frac{1}{2}(1+\zeta)\ ,\ \zeta^{-}=\frac{1}{2}(1-\zeta)\ ,\ \underline{\mathbf{X}}=\begin{Bmatrix}\mathbf{X}_1\\ \vdots\\ \mathbf{X}_{18}\end{Bmatrix}\ ,\ \underline{\mathbf{U}}=\begin{Bmatrix}\mathbf{U}_1\\ \vdots\\ \mathbf{U}_{18}\end{Bmatrix} \qquad (2)$$

and the interpolation matrices $\mathbb{N}$'s are self-defined. Without losing generality, z is aligned with the transverse or thickness direction of the shell being modeled. Same as the stress-resultant shell approach, the Jacobian determinant J is approximated by the one evaluated at the mid-surface for higher computational efficiency [19,27], i.e.

$$J = \det[\mathbf{X}_{\xi}, \mathbf{X}_{\eta}, \mathbf{X}_{\zeta}]\Big|_{\zeta=0}$$

The natural Green strain component ε_{ij}'s are :

$$\varepsilon_{ab} = (\mathbf{X}_{,a}^{T}\mathbf{U}_{,b} + \mathbf{X}_{,b}^{T}\mathbf{U}_{,a})/2 + (\mathbf{U}_{,a}^{T}\mathbf{U}_{,b} + \mathbf{U}_{,b}^{T}\mathbf{U}_{,a})/4 \tag{3}$$

in which a and b are natural coordinates. It can be seen that $\varepsilon_{\zeta\zeta}$ is independent of ζ and this feature leads to the thickness locking [15,21,22,26]. To resolve the problem in the present stabilized element whose core constituents are integrated by the 2×2 quadrature in the ξ-η-plane, it would be sufficient to incorporate the following four EAS modes which are linear in ζ :

$$\varepsilon_{\zeta\zeta}^{EAS} = \frac{\zeta}{J}\begin{bmatrix}1 & \xi & \eta & \xi\eta\end{bmatrix}\begin{Bmatrix}\lambda_1 \\ \vdots \\ \lambda_4\end{Bmatrix} = \zeta\mathbb{Q}\boldsymbol{\lambda} \tag{4}$$

in which the shape function matrix $\mathbb{Q}$ and the vector of coefficients $\boldsymbol{\lambda}$ are self-defined. The reciprocal of J is essential to secure the patch test fulfillment [1,15]. The vector of strain components derived from the displacement and the EAS modes with respect to an orthogonal coordinate system (x'y'z') can be expressed as :

$$\boldsymbol{\epsilon} = \{\varepsilon_{x'x'}, \varepsilon_{y'y'}, \varepsilon_{z'z'}, 2\varepsilon_{x'y'}, 2\varepsilon_{z'x'}, 2\varepsilon_{y'z'}\}^{T} = \mathbf{T}\{\varepsilon_{\xi\xi}, \varepsilon_{\xi\xi}, \varepsilon_{\zeta\zeta}, 2\varepsilon_{\xi\eta}, 2\varepsilon_{\zeta\xi}, 2\varepsilon_{\zeta\eta}\}^{T} \tag{5}$$

in which $\mathbf{T}$ is the transformation matrix. If it is assumed as usual that the z'-axis and the x'-y'-plane are parallel to respectively the ζ-axis and mid-surface of the shell,

$$\mathbf{T} = \begin{bmatrix} (x'_{\xi})^2 & (x'_{\eta})^2 & 0 & 2x'_{\xi}x'_{\eta} & 0 & 0 \\ (y'_{\xi})^2 & (y'_{\eta})^2 & 0 & 2y'_{\xi}y'_{\eta} & 0 & 0 \\ 0 & 0 & (z'_{\zeta})^2 & 0 & 0 & 0 \\ x'_{\xi}y'_{\xi} & x'_{\eta}y'_{\eta} & 0 & x'_{\xi}y'_{\eta} + x'_{\eta}y'_{\xi} & 0 & 0 \\ 0 & 0 & 0 & 0 & z'_{\zeta}x'_{\xi} & z'_{\zeta}x'_{\eta} \\ 0 & 0 & 0 & 0 & z'_{\zeta}y'_{\xi} & z'_{\zeta}y'_{\eta} \end{bmatrix}^{-T} \tag{6}$$

where

$x'_{\xi} = \mathbf{i}_{x'}^{T}\mathbf{X}_{o,\xi}$, $y'_{\xi} = \mathbf{i}_{y'}^{T}\mathbf{X}_{o,\xi}$, $x'_{\eta} = \mathbf{i}_{x'}^{T}\mathbf{X}_{o,\eta}$, $y'_{\eta} = \mathbf{i}_{y'}^{T}\mathbf{X}_{o,\eta}$, $z'_{\zeta} = \mathbf{i}_{z'}^{T}\mathbf{X}_{n}$,

$\mathbf{i}_{x'}$, $\mathbf{i}_{y'}$ and $\mathbf{i}_{z'}$ are respectively the unit vectors along the local x'-, y'- and z'-axes.

By retaining only the zero and first order ζ-terms, the vector of strain components in (5) can be expressed as :

$$\boldsymbol{\epsilon} = \boldsymbol{\epsilon}_o + \zeta\boldsymbol{\epsilon}_n = (\mathbb{B}_o^{\mathbf{X}+\mathbf{U}/2} + \zeta\mathbb{B}_n^{\mathbf{X}+\mathbf{U}/2})\begin{Bmatrix}\underline{\mathbf{U}}\\ \boldsymbol{\lambda}\end{Bmatrix} \tag{7}$$

where

$$\mathbb{B}_o^{\mathbf{X}} = \mathbf{T}\begin{bmatrix} \underline{\mathbf{X}}^T\mathbb{N}_{o,\xi}^T\mathbb{N}_{o,\xi} & \mathbf{0}\\ \underline{\mathbf{X}}^T\mathbb{N}_{o,\eta}^T\mathbb{N}_{o,\eta} & \mathbf{0}\\ \underline{\mathbf{X}}^T\mathbb{N}_n^T\mathbb{N}_n & \mathbf{0}\\ \underline{\mathbf{X}}^T(\mathbb{N}_{o,\xi}^T\mathbb{N}_{o,\eta} + \mathbb{N}_{o,\eta}^T\mathbb{N}_{o,\xi}) & \mathbf{0}\\ \underline{\mathbf{X}}^T(\mathbb{N}_n^T\mathbb{N}_{o,\xi} + \mathbb{N}_{o,\xi}^T\mathbb{N}_n) & \mathbf{0}\\ \underline{\mathbf{X}}^T(\mathbb{N}_n^T\mathbb{N}_{o,\eta} + \mathbb{N}_{o,\eta}^T\mathbb{N}_n) & \mathbf{0}\end{bmatrix},$$

$$\mathbb{B}_n^{\mathbf{X}} = \mathbf{T}\begin{bmatrix} \underline{\mathbf{X}}^T(\mathbb{N}_{n,\xi}^T\mathbb{N}_{o,\xi} + \mathbb{N}_{o,\xi}^T\mathbb{N}_{n,\xi}) & \mathbf{0}\\ \underline{\mathbf{X}}^T(\mathbb{N}_{n,\eta}^T\mathbb{N}_{o,\eta} + \mathbb{N}_{o,\eta}^T\mathbb{N}_{n,\eta}) & \mathbf{0}\\ \mathbf{0} & \mathbb{Q}\\ \underline{\mathbf{X}}^T(\mathbb{N}_{o,\eta}^T\mathbb{N}_{n,\xi} + \mathbb{N}_{o,\xi}^T\mathbb{N}_{n,\eta} + \mathbb{N}_{n,\xi}^T\mathbb{N}_{o,\eta} + \mathbb{N}_{n,\eta}^T\mathbb{N}_{o,\xi}) & \mathbf{0}\\ \underline{\mathbf{X}}^T(\mathbb{N}_n^T\mathbb{N}_{n,\xi} + \mathbb{N}_{n,\xi}^T\mathbb{N}_n) & \mathbf{0}\\ \underline{\mathbf{X}}^T(\mathbb{N}_n^T\mathbb{N}_{n,\eta} + \mathbb{N}_{n,\eta}^T\mathbb{N}_n) & \mathbf{0}\end{bmatrix}$$

For convenience, $\boldsymbol{\epsilon}$ will be termed as the enhanced displacement-derived strain.

3. LOWER AND HIGHER ORDER HYBRID STRAIN MODES

Besides thickness locking, the element is also plagued by shear and membrane lockings. To resolve them, a stabilization approach formulated by using the following hybrid-strain field denoted as $\mathbf{e}$ will be adopted [18,19] :

$$\mathbf{e} = \begin{bmatrix}\mathbf{I}_6 & \zeta\mathbf{I}_6\end{bmatrix}\begin{Bmatrix}\mathbf{e}_o\\ \mathbf{e}_n\end{Bmatrix} = \begin{bmatrix}\mathbf{I}_6 & \zeta\mathbf{I}_6\end{bmatrix}\begin{Bmatrix}\mathbb{P}_l\boldsymbol{\beta}_{ol} + \mathbb{P}_h\boldsymbol{\beta}_{oh}\\ \mathbb{P}_l\boldsymbol{\beta}_{nl} + \mathbb{P}_h\boldsymbol{\beta}_{nh}\end{Bmatrix} \tag{8}$$

where

$$\mathbb{P}_l = \frac{1}{4}\Big[(1-\xi\sqrt{3})(1-\eta\sqrt{3})\mathbf{I}_6\,,\,(1+\xi\sqrt{3})(1-\eta\sqrt{3})\mathbf{I}_6\,,\,(1+\xi\sqrt{3})(1+\eta\sqrt{3})\mathbf{I}_6\,,\,(1-\xi\sqrt{3})(1+\eta\sqrt{3})\mathbf{I}_6\Big]$$

is the lower order shape function matrix, $\boldsymbol{\beta}$'s are the vectors of coefficients, subscript "l" refers lower order and subscript "h" refers higher order. It will be shown that lower order modes will lead

to the uniformly reduced integrated element. In this light, the higher order modes are chosen to suppress the compatible zero energy modes which can propagate among the element mesh. For a geometric regular and uniformly reduced integrated (by the 2×2 quadrature in the ξ-η-plane) element, the linear strain derived from compatible zero energy modes are [21,24] :

$$\begin{Bmatrix} \varepsilon_{\xi\xi} \\ \varepsilon_{\eta\eta} \\ \varepsilon_{\zeta\zeta} \\ 2\varepsilon_{\zeta\eta} \\ 2\varepsilon_{\zeta\xi} \\ 2\varepsilon_{\xi\eta} \end{Bmatrix} = \begin{bmatrix} 2p_{\xi} & 2\zeta p_{\xi} & 0 & 0 & 0 & 0 \\ 0 & 0 & 2p_{\eta} & 2\zeta p_{\eta} & 0 & 0 \\ 0 & 0 & 0 & 0 & 0 & p_{\xi\eta} \\ 0 & 0 & 0 & p_{\xi\eta} & 2p_{\eta} & 2\zeta p_{\eta} \\ 0 & p_{\xi\eta} & 0 & 0 & 2p_{\xi} & 2\zeta p_{\xi} \\ 2p_{\eta} & 2\zeta p_{\eta} & 2p_{\xi} & 2\zeta p_{\xi} & 0 & 0 \end{bmatrix} \begin{Bmatrix} c_1 \\ c_2 \\ c_3 \\ c_4 \\ c_5 \\ c_6 \end{Bmatrix} \tag{9}$$

in which $p_{\xi} = \xi(3\eta^2 - 1)$, $p_{\eta} = \eta(3\xi^2 - 1)$ and $p_{\xi\eta} = \xi\eta(3\xi^2 - 1)(3\eta^2 - 1)$. Based on the above matrix, the following higher order strain matrix is chosen :

$$\mathbb{P}_h = \frac{1}{J}(\bar{\mathbf{C}}\mathbf{T})^{-1} \begin{bmatrix} p_{\xi} & 0 & 0 \\ 0 & p_{\eta} & 0 \\ 0 & 0 & 0 \\ 0 & 0 & 0 \\ 0 & 0 & p_{\xi} \\ 0 & 0 & p_{\eta} \end{bmatrix} \tag{10}$$

in which $\bar{\mathbf{C}}$ is the tangential material stiffness matrix at zero strain and the reciprocal of J is essential to secure the patch test fulfillment [28]. As a matter of fact, $\mathbb{P}_l$ and $\mathbb{P}_h$ also possess certain orthogonal properties that will be discussed later on.

4. WEAK FORMS

Let (**U**,**λ**,**e**) be an acquired approximate solution to the static equilibrium problem and (**U**+Δ**U**, **λ**+Δ**λ**,**e**+Δ**e**) be the refined or better approximate solution. The present task is to evaluate the refinement or increment (Δ**U**,Δ**λ**,Δ**e**). The following weak forms can be used [19] :

$$\int_{\Omega^e} (\boldsymbol{\epsilon} + \Delta\boldsymbol{\epsilon} - \mathbf{e} - \Delta\mathbf{e})^T \mathbf{C}\delta\Delta\mathbf{e} d\Omega = 0 \tag{11}$$

$$\sum_e \delta U^e = \delta W \tag{12}$$

where Ω^e denotes the element domain in its initial configuration, δ is the virtual symbol and δW is the external virtual work. Moreover,

$$\delta U^e = \int_{\Omega^e} (\boldsymbol{\sigma} + \mathbf{C}\Delta\mathbf{e})^T \delta\Delta\boldsymbol{\epsilon} d\Omega \tag{13}$$

is the elementwise internal virtual work. For hyperelastic materials, the vector of second Piola-Kirchhoff stress components $\boldsymbol{\sigma}$ and tangential material stiffness matrix $\mathbf{C}$ can be derived from the strain energy function $A(\mathbf{e})$ as :

$$\boldsymbol{\sigma} = \left.\frac{\partial A}{\partial \mathbf{e}}\right|_{\mathbf{e}} , \ \mathbf{C} = \left.\frac{\partial}{\partial \mathbf{e}}\left(\frac{\partial A}{\partial \mathbf{e}}\right)^T\right|_{\mathbf{e}} \tag{14}$$

It can be seen that (11) enforces the equality of the refined enhanced displacement-derived strain $\boldsymbol{\epsilon}+\Delta\boldsymbol{\epsilon}$ and the refined hybrid strain $\mathbf{e}+\Delta\mathbf{e}$. On the other hand, (12) is the virtual work statement which enforces the stress equilibrium and traction boundary conditions. Noting that the incremental strains arise from $\Delta\mathbf{U}$, $\Delta\boldsymbol{\lambda}$ and $\Delta\boldsymbol{\beta}$'s, (7) and (8) lead to :

$$\begin{aligned}
&\Delta\boldsymbol{\epsilon} = \Delta\boldsymbol{\epsilon}_o + \zeta\Delta\boldsymbol{\epsilon}_n = \begin{bmatrix}\mathbf{I}_6 & \zeta\mathbf{I}_6\end{bmatrix}\begin{bmatrix}\mathbb{B}_o^{\mathbf{X}+\mathbf{U}+\Delta\mathbf{U}/2} \\ \mathbb{B}_n^{\mathbf{X}+\mathbf{U}+\Delta\mathbf{U}/2}\end{bmatrix}\begin{Bmatrix}\Delta\underline{\mathbf{U}} \\ \Delta\boldsymbol{\lambda}\end{Bmatrix} = \begin{bmatrix}\mathbf{I}_6 & \zeta\mathbf{I}_6\end{bmatrix}\begin{bmatrix}\mathbb{B}_o^{\mathbf{X}+\mathbf{U}} + \mathbb{B}_o^{\Delta\mathbf{U}/2} \\ \mathbb{B}_n^{\mathbf{X}+\mathbf{U}} + \mathbb{B}_n^{\Delta\mathbf{U}/2}\end{bmatrix}\begin{Bmatrix}\Delta\underline{\mathbf{U}} \\ \Delta\boldsymbol{\lambda}\end{Bmatrix}, \\
&\delta\Delta\boldsymbol{\epsilon} = \delta\Delta\boldsymbol{\epsilon}_o + \zeta\delta\Delta\boldsymbol{\epsilon}_n = \begin{bmatrix}\mathbf{I}_6 & \zeta\mathbf{I}_6\end{bmatrix}\begin{bmatrix}\mathbb{B}_o^{\mathbf{X}+\mathbf{U}+\Delta\mathbf{U}} \\ \mathbb{B}_n^{\mathbf{X}+\mathbf{U}+\Delta\mathbf{U}}\end{bmatrix}\begin{Bmatrix}\delta\Delta\underline{\mathbf{U}} \\ \delta\Delta\boldsymbol{\lambda}\end{Bmatrix} = \begin{bmatrix}\mathbf{I}_6 & \zeta\mathbf{I}_6\end{bmatrix}\begin{bmatrix}\mathbb{B}_o^{\mathbf{X}+\mathbf{U}} + \mathbb{B}_o^{\Delta\mathbf{U}} \\ \mathbb{B}_n^{\mathbf{X}+\mathbf{U}} + \mathbb{B}_n^{\Delta\mathbf{U}}\end{bmatrix}\begin{Bmatrix}\delta\Delta\underline{\mathbf{U}} \\ \delta\Delta\boldsymbol{\lambda}\end{Bmatrix}, \\
&\Delta\mathbf{e} = \begin{bmatrix}\mathbf{I}_6 & \zeta\mathbf{I}_6\end{bmatrix}\begin{Bmatrix}\mathbb{P}_l\,\Delta\boldsymbol{\beta}_{ol} + \mathbb{P}_h\,\Delta\boldsymbol{\beta}_{oh} \\ \mathbb{P}_l\,\Delta\boldsymbol{\beta}_{nl} + \mathbb{P}_h\,\Delta\boldsymbol{\beta}_{nh}\end{Bmatrix}, \ \delta\Delta\mathbf{e} = \begin{bmatrix}\mathbf{I}_6 & \zeta\mathbf{I}_6\end{bmatrix}\begin{Bmatrix}\mathbb{P}_l\,\delta\Delta\boldsymbol{\beta}_{ol} + \mathbb{P}_h\,\delta\Delta\boldsymbol{\beta}_{oh} \\ \mathbb{P}_l\,\delta\Delta\boldsymbol{\beta}_{nl} + \mathbb{P}_h\,\delta\Delta\boldsymbol{\beta}_{nh}\end{Bmatrix}
\end{aligned} \tag{15}$$

After invoking (15) as well as linearizing with respect to the incremental terms, (11) and (13) become :

$$\left\langle \begin{Bmatrix}\mathbb{P}_l\delta\Delta\boldsymbol{\beta}_{ol} + \mathbb{P}_h\delta\Delta\boldsymbol{\beta}_{oh} \\ \mathbb{P}_l\delta\Delta\boldsymbol{\beta}_{nl} + \mathbb{P}_h\delta\Delta\boldsymbol{\beta}_{nh}\end{Bmatrix}^T \begin{bmatrix}\mathbf{C}_0 & \mathbf{C}_1 \\ \mathbf{C}_1 & \mathbf{C}_2\end{bmatrix}\left(\begin{Bmatrix}\boldsymbol{\epsilon}_o - \mathbf{e}_o \\ \boldsymbol{\epsilon}_n - \mathbf{e}_n\end{Bmatrix} + \begin{bmatrix}\mathbb{B}_o^{\mathbf{X}+\mathbf{U}} \\ \mathbb{B}_n^{\mathbf{X}+\mathbf{U}}\end{bmatrix}\begin{Bmatrix}\Delta\underline{\mathbf{U}} \\ \Delta\boldsymbol{\lambda}\end{Bmatrix} - \begin{Bmatrix}\mathbb{P}_l\Delta\boldsymbol{\beta}_{ol} + \mathbb{P}_h\Delta\boldsymbol{\beta}_{oh} \\ \mathbb{P}_l\Delta\boldsymbol{\beta}_{nl} + \mathbb{P}_h\Delta\boldsymbol{\beta}_{nh}\end{Bmatrix}\right)\right\rangle = \mathbf{0} \tag{16}$$

$$\delta U^e = \begin{Bmatrix}\delta\Delta\underline{\mathbf{U}} \\ \delta\Delta\boldsymbol{\lambda}\end{Bmatrix}\left\langle \begin{bmatrix}\mathbb{B}_o^{\mathbf{X}+\mathbf{U}+\Delta\mathbf{U}} \\ \mathbb{B}_n^{\mathbf{X}+\mathbf{U}+\Delta\mathbf{U}}\end{bmatrix}^T \begin{Bmatrix}\boldsymbol{\sigma}_o \\ \boldsymbol{\sigma}_n\end{Bmatrix} + \begin{bmatrix}\mathbb{B}_o^{\mathbf{X}+\mathbf{U}} \\ \mathbb{B}_n^{\mathbf{X}+\mathbf{U}}\end{bmatrix}^T \begin{bmatrix}\mathbf{C}_0 & \mathbf{C}_1 \\ \mathbf{C}_1 & \mathbf{C}_2\end{bmatrix}\begin{Bmatrix}\Delta\mathbf{e}_o \\ \Delta\mathbf{e}_n\end{Bmatrix}\right\rangle \tag{17}$$

where

$$\langle f(\xi,\eta)\rangle = \int_{-1}^{+1}\int_{-1}^{+1} f(\xi,\eta) J d\xi d\eta \ , \ \begin{bmatrix}\mathbf{C}_0 & \mathbf{C}_1 \\ \mathbf{C}_1 & \mathbf{C}_2\end{bmatrix} = \int_{-1}^{+1}\begin{bmatrix}\mathbf{C} & \zeta\mathbf{C} \\ \zeta\mathbf{C} & \zeta^2\mathbf{C}\end{bmatrix} d\zeta \ , \ \begin{Bmatrix}\boldsymbol{\sigma}_o \\ \boldsymbol{\sigma}_n\end{Bmatrix} = \int_{-1}^{+1}\begin{Bmatrix}\boldsymbol{\sigma} \\ \zeta\boldsymbol{\sigma}\end{Bmatrix} d\zeta .$$

Under the standard order of integration which is the lowest order numerical integration rule that can preserve the rank of the matrix being evaluated [29], the following orthogonal properties between $\mathbb{P}_l$ and $\mathbb{P}_h$ are valid :

$$\langle \mathbb{P}_l^T \mathbf{C}_0 \mathbb{P}_h \rangle_L = \langle \mathbb{P}_l^T \mathbf{C}_1 \mathbb{P}_h \rangle_L = \langle \mathbb{P}_l^T \mathbf{C}_2 \mathbb{P}_h \rangle_L = \mathbf{0} \tag{18}$$

in which $\langle f \rangle_L$ denotes the integral of fJ evaluated by using the 2×2 quadrature in the ξ-η-plane. Thus, (16) can be expanded as :

$$\sum_{\Theta=l,h} \langle \begin{Bmatrix} \mathbb{P}_\Theta \delta\Delta\boldsymbol{\beta}_{o\Theta} \\ \mathbb{P}_\Theta \delta\Delta\boldsymbol{\beta}_{n\Theta} \end{Bmatrix}^T \begin{bmatrix} \mathbf{C}_0 & \mathbf{C}_1 \\ \mathbf{C}_1 & \mathbf{C}_2 \end{bmatrix} (\begin{Bmatrix} \boldsymbol{\epsilon}_o - \mathbf{e}_o \\ \boldsymbol{\epsilon}_n - \mathbf{e}_n \end{Bmatrix} + \begin{bmatrix} \mathbb{B}_o^{\mathbf{X}+\mathbf{U}} \\ \mathbb{B}_n^{\mathbf{X}+\mathbf{U}} \end{bmatrix} \begin{Bmatrix} \Delta\underline{\mathbf{U}} \\ \Delta\boldsymbol{\lambda} \end{Bmatrix} - \begin{Bmatrix} \mathbb{P}_\Theta \Delta\boldsymbol{\beta}_{o\Theta} \\ \mathbb{P}_\Theta \Delta\boldsymbol{\beta}_{n\Theta} \end{Bmatrix}) \rangle = 0 \quad \text{for} \quad \Theta = l,h \tag{19}$$

or, equivalently,

$$\begin{Bmatrix} \Delta\boldsymbol{\beta}_{o\Theta} \\ \Delta\boldsymbol{\beta}_{n\Theta} \end{Bmatrix} = \mathbb{G}_\Theta \begin{Bmatrix} \Delta\underline{\mathbf{U}} \\ \Delta\boldsymbol{\lambda} \end{Bmatrix} + \mathbb{H}_\Theta^{-1} \mathbf{Z}_\Theta \qquad \text{for} \quad \Theta = l,h \tag{20}$$

where

$$\mathbb{H}_\Theta = \langle \begin{bmatrix} \mathbb{P}_\Theta^T \mathbf{C}_0 \mathbb{P}_\Theta & \mathbb{P}_\Theta^T \mathbf{C}_1 \mathbb{P}_\Theta \\ \mathbb{P}_\Theta^T \mathbf{C}_1 \mathbb{P}_\Theta & \mathbb{P}_\Theta^T \mathbf{C}_2 \mathbb{P}_\Theta \end{bmatrix} \rangle \ , \ \mathbb{G}_\Theta = \langle \begin{bmatrix} \mathbb{P}_\Theta^T \mathbf{C}_0 & \mathbb{P}_\Theta^T \mathbf{C}_1 \\ \mathbb{P}_\Theta^T \mathbf{C}_1 & \mathbb{P}_\Theta^T \mathbf{C}_2 \end{bmatrix} \begin{bmatrix} \mathbb{B}_o^{\mathbf{X}+\mathbf{U}} \\ \mathbb{B}_n^{\mathbf{X}+\mathbf{U}} \end{bmatrix} \rangle \ ,$$

$$\mathbf{Z}_\Theta = \langle \begin{bmatrix} \mathbb{P}_\Theta^T \mathbf{C}_0 & \mathbb{P}_\Theta^T \mathbf{C}_1 \\ \mathbb{P}_\Theta^T \mathbf{C}_1 & \mathbb{P}_\Theta^T \mathbf{C}_2 \end{bmatrix} \begin{Bmatrix} \boldsymbol{\epsilon}_o - \mathbf{e}_o \\ \boldsymbol{\epsilon}_n - \mathbf{e}_n \end{Bmatrix} \rangle .$$

Substitution of (15) and (20) into (17) results in :

$$\delta U^e = \begin{Bmatrix} \delta\Delta\underline{\mathbf{U}} \\ \delta\Delta\boldsymbol{\lambda} \end{Bmatrix} [\langle \begin{bmatrix} \mathbb{B}_o^{\mathbf{X}+\mathbf{U}+\Delta\mathbf{U}} \\ \mathbb{B}_n^{\mathbf{X}+\mathbf{U}+\Delta\mathbf{U}} \end{bmatrix}^T \begin{Bmatrix} \boldsymbol{\sigma}_o \\ \boldsymbol{\sigma}_n \end{Bmatrix} \rangle + \sum_{\Theta=l,h} (\mathbb{G}_\Theta^T \mathbb{H}_\Theta^{-1} \mathbb{G}_\Theta \begin{Bmatrix} \Delta\underline{\mathbf{U}} \\ \Delta\boldsymbol{\lambda} \end{Bmatrix} + \mathbb{G}_\Theta^T \mathbb{H}_\Theta^{-1} \mathbf{Z}_\Theta)] \tag{21}$$

5. FURTHER MANIPULATIONS AND SIMPLICATIONS

The standard order integration rule for $\mathbb{G}_l$, $\mathbf{Z}_l$ and $\mathbb{H}_l$ is the 2×2 quadrature using which and recalling (20), it can be shown that

$$\mathbb{G}_l = \begin{bmatrix} (\mathbf{C}_0\mathbb{B}_o^{\mathbf{X}+\mathbf{U}} + \mathbf{C}_1\mathbb{B}_n^{\mathbf{X}+\mathbf{U}})_1 \\ (\mathbf{C}_0\mathbb{B}_o^{\mathbf{X}+\mathbf{U}} + \mathbf{C}_1\mathbb{B}_n^{\mathbf{X}+\mathbf{U}})_2 \\ (\mathbf{C}_0\mathbb{B}_o^{\mathbf{X}+\mathbf{U}} + \mathbf{C}_1\mathbb{B}_n^{\mathbf{X}+\mathbf{U}})_3 \\ (\mathbf{C}_0\mathbb{B}_o^{\mathbf{X}+\mathbf{U}} + \mathbf{C}_1\mathbb{B}_n^{\mathbf{X}+\mathbf{U}})_4 \\ (\mathbf{C}_1\mathbb{B}_o^{\mathbf{X}+\mathbf{U}} + \mathbf{C}_2\mathbb{B}_n^{\mathbf{X}+\mathbf{U}})_1 \\ (\mathbf{C}_1\mathbb{B}_o^{\mathbf{X}+\mathbf{U}} + \mathbf{C}_2\mathbb{B}_n^{\mathbf{X}+\mathbf{U}})_2 \\ (\mathbf{C}_1\mathbb{B}_o^{\mathbf{X}+\mathbf{U}} + \mathbf{C}_2\mathbb{B}_n^{\mathbf{X}+\mathbf{U}})_3 \\ (\mathbf{C}_1\mathbb{B}_o^{\mathbf{X}+\mathbf{U}} + \mathbf{C}_2\mathbb{B}_n^{\mathbf{X}+\mathbf{U}})_4 \end{bmatrix}, \quad \mathbf{Z}_l = \begin{bmatrix} \left(\mathbf{C}_0(\boldsymbol{\epsilon}_o - \mathbf{e}_o) + \mathbf{C}_1(\boldsymbol{\epsilon}_n - \mathbf{e}_n)\right)_1 \\ \left(\mathbf{C}_0(\boldsymbol{\epsilon}_o - \mathbf{e}_o) + \mathbf{C}_1(\boldsymbol{\epsilon}_n - \mathbf{e}_n)\right)_2 \\ \left(\mathbf{C}_0(\boldsymbol{\epsilon}_o - \mathbf{e}_o) + \mathbf{C}_1(\boldsymbol{\epsilon}_n - \mathbf{e}_n)\right)_3 \\ \left(\mathbf{C}_0(\boldsymbol{\epsilon}_o - \mathbf{e}_o) + \mathbf{C}_1(\boldsymbol{\epsilon}_n - \mathbf{e}_n)\right)_4 \\ \left(\mathbf{C}_1(\boldsymbol{\epsilon}_o - \mathbf{e}_o) + \mathbf{C}_2(\boldsymbol{\epsilon}_n - \mathbf{e}_n)\right)_1 \\ \left(\mathbf{C}_1(\boldsymbol{\epsilon}_o - \mathbf{e}_o) + \mathbf{C}_2(\boldsymbol{\epsilon}_n - \mathbf{e}_n)\right)_2 \\ \left(\mathbf{C}_1(\boldsymbol{\epsilon}_o - \mathbf{e}_o) + \mathbf{C}_2(\boldsymbol{\epsilon}_n - \mathbf{e}_n)\right)_3 \\ \left(\mathbf{C}_1(\boldsymbol{\epsilon}_o - \mathbf{e}_o) + \mathbf{C}_2(\boldsymbol{\epsilon}_n - \mathbf{e}_n)\right)_4 \end{bmatrix},$$

$$\mathbb{H}_l = \begin{bmatrix} (\mathbf{C}_0)_1 & \mathbf{0}_{6\times6} & \mathbf{0}_{6\times6} & \mathbf{0}_{6\times6} & (\mathbf{C}_1)_1 & \mathbf{0}_{6\times6} & \mathbf{0}_{6\times6} & \mathbf{0}_{6\times6} \\ \mathbf{0}_{6\times6} & (\mathbf{C}_0)_2 & \mathbf{0}_{6\times6} & \mathbf{0}_{6\times6} & \mathbf{0}_{6\times6} & (\mathbf{C}_1)_2 & \mathbf{0}_{6\times6} & \mathbf{0}_{6\times6} \\ \mathbf{0}_{6\times6} & \mathbf{0}_{6\times6} & (\mathbf{C}_0)_3 & \mathbf{0}_{6\times6} & \mathbf{0}_{6\times6} & \mathbf{0}_{6\times6} & (\mathbf{C}_1)_3 & \mathbf{0}_{6\times6} \\ \mathbf{0}_{6\times6} & \mathbf{0}_{6\times6} & \mathbf{0}_{6\times6} & (\mathbf{C}_0)_4 & \mathbf{0}_{6\times6} & \mathbf{0}_{6\times6} & \mathbf{0}_{6\times6} & (\mathbf{C}_1)_4 \\ (\mathbf{C}_1)_1 & \mathbf{0}_{6\times6} & \mathbf{0}_{6\times6} & \mathbf{0}_{6\times6} & (\mathbf{C}_2)_1 & \mathbf{0}_{6\times6} & \mathbf{0}_{6\times6} & \mathbf{0}_{6\times6} \\ \mathbf{0}_{6\times6} & (\mathbf{C}_1)_2 & \mathbf{0}_{6\times6} & \mathbf{0}_{6\times6} & \mathbf{0}_{6\times6} & (\mathbf{C}_2)_2 & \mathbf{0}_{6\times6} & \mathbf{0}_{6\times6} \\ \mathbf{0}_{6\times6} & \mathbf{0}_{6\times6} & (\mathbf{C}_1)_3 & \mathbf{0}_{6\times6} & \mathbf{0}_{6\times6} & \mathbf{0}_{6\times6} & (\mathbf{C}_2)_3 & \mathbf{0}_{6\times6} \\ \mathbf{0}_{6\times6} & \mathbf{0}_{6\times6} & \mathbf{0}_{6\times6} & (\mathbf{C}_1)_4 & \mathbf{0}_{6\times6} & \mathbf{0}_{6\times6} & \mathbf{0}_{6\times6} & (\mathbf{C}_2)_4 \end{bmatrix},$$

$$\begin{Bmatrix} \Delta\boldsymbol{\beta}_{ol} \\ \Delta\boldsymbol{\beta}_{nl} \end{Bmatrix} = \mathbb{H}_l^{-1}(\mathbb{G}_l \begin{Bmatrix} \Delta\underline{\mathbf{U}} \\ \Delta\boldsymbol{\lambda} \end{Bmatrix} + \mathbf{Z}_l) = \begin{bmatrix} (\mathbb{B}_o^{\mathbf{X}+\mathbf{U}})_1 \\ (\mathbb{B}_o^{\mathbf{X}+\mathbf{U}})_2 \\ (\mathbb{B}_o^{\mathbf{X}+\mathbf{U}})_3 \\ (\mathbb{B}_o^{\mathbf{X}+\mathbf{U}})_4 \\ (\mathbb{B}_n^{\mathbf{X}+\mathbf{U}})_1 \\ (\mathbb{B}_n^{\mathbf{X}+\mathbf{U}})_2 \\ (\mathbb{B}_n^{\mathbf{X}+\mathbf{U}})_3 \\ (\mathbb{B}_n^{\mathbf{X}+\mathbf{U}})_4 \end{bmatrix} \begin{Bmatrix} \Delta\underline{\mathbf{U}} \\ \Delta\boldsymbol{\lambda} \end{Bmatrix} + \begin{bmatrix} (\boldsymbol{\epsilon}_o - \mathbf{e}_o)_1 \\ (\boldsymbol{\epsilon}_o - \mathbf{e}_o)_2 \\ (\boldsymbol{\epsilon}_o - \mathbf{e}_o)_3 \\ (\boldsymbol{\epsilon}_o - \mathbf{e}_o)_4 \\ (\boldsymbol{\epsilon}_n - \mathbf{e}_n)_1 \\ (\boldsymbol{\epsilon}_n - \mathbf{e}_n)_2 \\ (\boldsymbol{\epsilon}_n - \mathbf{e}_n)_3 \\ (\boldsymbol{\epsilon}_n - \mathbf{e}_n)_4 \end{bmatrix},$$

$$(\Delta\mathbf{e}_o)_i = (\mathbb{P}_l)_i \Delta\boldsymbol{\beta}_{ol} = (\mathbb{B}_o^{\mathbf{X}+\mathbf{U}} \begin{Bmatrix} \Delta\underline{\mathbf{U}} \\ \Delta\boldsymbol{\lambda} \end{Bmatrix} + \boldsymbol{\epsilon}_o - \mathbf{e}_o)_i \ , \ (\Delta\mathbf{e}_n)_i = (\mathbb{P}_l)_i \Delta\boldsymbol{\beta}_{nl} = (\mathbb{B}_n^{\mathbf{X}+\mathbf{U}} \begin{Bmatrix} \Delta\underline{\mathbf{U}} \\ \Delta\boldsymbol{\lambda} \end{Bmatrix} + \boldsymbol{\epsilon}_n - \mathbf{e}_n)_i \ ,$$

$$\mathbb{G}_l^T\mathbb{H}_l^{-1}\mathbb{G}_l = \langle \begin{bmatrix} \mathbb{B}_o^{\mathbf{X}+\mathbf{U}} \\ \mathbb{B}_n^{\mathbf{X}+\mathbf{U}} \end{bmatrix}^T \begin{bmatrix} \mathbf{C}_0 & \mathbf{C}_1 \\ \mathbf{C}_1 & \mathbf{C}_2 \end{bmatrix} \begin{bmatrix} \mathbb{B}_o^{\mathbf{X}+\mathbf{U}} \\ \mathbb{B}_n^{\mathbf{X}+\mathbf{U}} \end{bmatrix} \rangle_L \ , \ \mathbb{G}_l^T\mathbb{H}_l^{-1}\mathbf{Z}_l = \langle \begin{bmatrix} \mathbb{B}_o^{\mathbf{X}+\mathbf{U}} \\ \mathbb{B}_n^{\mathbf{X}+\mathbf{U}} \end{bmatrix}^T \begin{bmatrix} \mathbf{C}_0 & \mathbf{C}_1 \\ \mathbf{C}_1 & \mathbf{C}_2 \end{bmatrix} \begin{Bmatrix} \boldsymbol{\epsilon}_o - \mathbf{e}_o \\ \boldsymbol{\epsilon}_n - \mathbf{e}_n \end{Bmatrix} \rangle_L \quad (22)$$

where $()_i$ denotes the value of the braced term at the i-th sampling point of the 2×2 quadrature. Furthermore, if $\mathbf{Z}_h$ and the term involving the stresses in (21) are evaluated by the 2×2 quadrature,

$$\mathbf{Z}_h = \mathbf{0} \ , \ \langle \begin{bmatrix} \mathbb{B}_o^{\mathbf{X}+\mathbf{U}+\Delta\mathbf{U}} \\ \mathbb{B}_n^{\mathbf{X}+\mathbf{U}+\Delta\mathbf{U}} \end{bmatrix}^T \begin{Bmatrix} \boldsymbol{\sigma}_o \\ \boldsymbol{\sigma}_n \end{Bmatrix} \rangle_L + \mathbb{G}_l^T\mathbb{H}_l^{-1}\mathbf{Z}_l = \underline{\mathbf{Q}} + \mathbb{K}_\sigma \begin{Bmatrix} \Delta\underline{\mathbf{U}} \\ \Delta\boldsymbol{\lambda} \end{Bmatrix} \quad (23)$$

where

$$\underline{\mathbf{Q}} = \langle \begin{bmatrix} \mathbb{B}_o^{\mathbf{X}+\mathbf{U}} \\ \mathbb{B}_n^{\mathbf{X}+\mathbf{U}} \end{bmatrix}^T (\begin{Bmatrix} \boldsymbol{\sigma}_o \\ \boldsymbol{\sigma}_n \end{Bmatrix} + \begin{bmatrix} \mathbf{C}_0 & \mathbf{C}_1 \\ \mathbf{C}_1 & \mathbf{C}_2 \end{bmatrix} \begin{Bmatrix} \boldsymbol{\epsilon}_o - \mathbf{e}_o \\ \boldsymbol{\epsilon}_n - \mathbf{e}_n \end{Bmatrix}) \rangle_l \ , \ \mathbb{K}_\sigma \begin{Bmatrix} \Delta\underline{\mathbf{U}} \\ \Delta\boldsymbol{\lambda} \end{Bmatrix} = \langle \begin{bmatrix} \mathbb{B}_o^{\Delta\mathbf{U}} \\ \mathbb{B}_n^{\Delta\mathbf{U}} \end{bmatrix}^T \begin{Bmatrix} \boldsymbol{\sigma}_o \\ \boldsymbol{\sigma}_n \end{Bmatrix} \rangle_l .$$

In the above equation, $\underline{\mathbf{Q}}$ represents the lumped nodal equivalent effect of the stress and the mismatch of the hybrid and enhanced displacement-derived strains whereas $\mathbb{K}_\sigma$ is the initial stress matrix. Substitution of (22) and (23) into (21) yields :

$$\delta U^e = \begin{Bmatrix} \delta\Delta\underline{\mathbf{U}} \\ \delta\Delta\boldsymbol{\lambda} \end{Bmatrix} (\underline{\mathbf{Q}} + \mathbb{K} \begin{Bmatrix} \Delta\underline{\mathbf{U}} \\ \Delta\boldsymbol{\lambda} \end{Bmatrix}) \tag{24}$$

where

$$\mathbb{K} = \mathbb{K}_\sigma + \langle \begin{bmatrix} \mathbb{B}_o^{\mathbf{X}+\mathbf{U}} \\ \mathbb{B}_n^{\mathbf{X}+\mathbf{U}} \end{bmatrix}^T \begin{bmatrix} \mathbf{C}_0 & \mathbf{C}_1 \\ \mathbf{C}_1 & \mathbf{C}_2 \end{bmatrix} \begin{bmatrix} \mathbb{B}_o^{\mathbf{X}+\mathbf{U}} \\ \mathbb{B}_n^{\mathbf{X}+\mathbf{U}} \end{bmatrix} \rangle_l + \mathbb{G}_h^T \mathbb{H}_h^{-1} \mathbb{G}_h$$

is the generalized tangential element stiffness matrix. Compared to the generalized tangential element stiffness matrix of the uniformly reduced integrated element, the only extra term in $\mathbb{K}$ is $\mathbb{G}_h^T \mathbb{H}_h^{-1} \mathbb{G}_h$ which plays the role of stabilizing the element. Noting that the number of higher order hybrid strain modes is 6 whereas total number of nodal d.o.f.s and EAS modes is 58, the accuracy of element is not sensitive to whether $\mathbb{H}_h$ and $\mathbb{G}_h$ are legitimately evaluated. In this light, the tangential material stiffness matrix is approximated by its strain-free counterpart, i.e. $\mathbf{C} \simeq \bar{\mathbf{C}} = \mathbf{C}\big|_{\mathbf{e}=\mathbf{0}}$. $\mathbb{G}_h$ and $\mathbb{H}_h$ can then be simplified to :

$$\mathbb{G}_h = 2 \int_{-1}^{+1} \int_{-1}^{+1} \begin{bmatrix} (\underline{\mathbf{X}} + \underline{\mathbf{U}})^T (p_\xi \mathbb{N}_{o,\xi}^T \mathbb{N}_{o,\xi}) & \mathbf{0}_{1\times4} \\ (\underline{\mathbf{X}} + \underline{\mathbf{U}})^T (p_\eta \mathbb{N}_{o,\eta}^T \mathbb{N}_{o,\eta}) & \mathbf{0}_{1\times4} \\ (\underline{\mathbf{X}} + \underline{\mathbf{U}})^T (p_\xi \mathbb{N}_n^T \mathbb{N}_{o,\xi} + p_\xi \mathbb{N}_{o,\xi}^T \mathbb{N}_n + p_\eta \mathbb{N}_n^T \mathbb{N}_{o,\eta} + p_\eta \mathbb{N}_{o,\eta}^T \mathbb{N}_n) & \mathbf{0}_{1\times4} \\ (\underline{\mathbf{X}} + \underline{\mathbf{U}})^T (p_\xi \mathbb{N}_{n,\xi}^T \mathbb{N}_{o,\xi} + p_\xi \mathbb{N}_{o,\xi}^T \mathbb{N}_{n,\xi})/3 & \mathbf{0}_{1\times4} \\ (\underline{\mathbf{X}} + \underline{\mathbf{U}})^T (p_\eta \mathbb{N}_{n,\eta}^T \mathbb{N}_{o,\eta} + p_\eta \mathbb{N}_{o,\eta}^T \mathbb{N}_{n,\eta})/3 & \mathbf{0}_{1\times4} \\ (\underline{\mathbf{X}} + \underline{\mathbf{U}})^T (p_\xi \mathbb{N}_n^T \mathbb{N}_{n,\xi} + p_\xi \mathbb{N}_{n,\xi}^T \mathbb{N}_n + p_\eta \mathbb{N}_n^T \mathbb{N}_{n,\eta} + p_\eta \mathbb{N}_{n,\eta}^T \mathbb{N}_n)/3 & \mathbf{0}_{1\times4} \end{bmatrix} d\xi d\eta$$

and

$$\mathbb{H}_H = \langle \frac{1}{J^2} \begin{bmatrix} \mathbb{P}^T \\ \zeta \mathbb{P}^T \end{bmatrix} \mathbf{S} \begin{bmatrix} \mathbb{P} & \zeta \mathbb{P} \end{bmatrix} \rangle = \langle \frac{1}{J^2} \begin{bmatrix} \mathbb{P}^T \mathbf{S} \mathbb{P} & \mathbf{0} \\ \mathbf{0} & \zeta^2 \mathbb{P}^T \mathbf{S} \mathbb{P} \end{bmatrix} \rangle \tag{25}$$

where

$$\mathbf{S} = [S_{ij}] = \mathbf{T}^{-T} \bar{\mathbf{C}}^{-1} \mathbf{T}^{-1},$$

$$\tilde{\mathbb{P}} = \begin{bmatrix} p_\xi & 0 & 0 \\ 0 & p_\eta & 0 \\ 0 & 0 & 0 \\ 0 & 0 & 0 \\ 0 & 0 & p_\xi \\ 0 & 0 & p_\eta \end{bmatrix} \quad ,$$

$$\mathbb{P}^T \mathbf{S} \mathbb{P} = \begin{bmatrix} p_\xi^2 S_{11} & p_\xi p_\eta S_{12} & p_\xi^2 S_{15} + p_\xi p_\eta S_{16} \\ p_\xi p_\eta S_{12} & p_\eta^2 S_{22} & p_\xi p_\eta S_{25} + p_\eta^2 S_{26} \\ p_\xi^2 S_{15} + p_\xi p_\eta S_{16} & p_\xi p_\eta S_{25} + p_\eta^2 S_{26} & p_\xi^2 S_{55} + 2 p_\xi p_\eta S_{56} + p_\eta^2 S_{66} \end{bmatrix}$$

When J is approximated by $J_o = J\big|_{\xi=\eta=0}$ in $\mathbb{H}_h$, the latter becomes

$$\mathbb{H}_H = \frac{64}{45 J_o} diag.\{ \begin{bmatrix} S_{11} & 0 & S_{15} \\ 0 & S_{22} & S_{26} \\ S_{15} & S_{26} & S_{55} + S_{66} \end{bmatrix}, \frac{1}{3} \begin{bmatrix} S_{11} & 0 & S_{15} \\ 0 & S_{22} & S_{26} \\ S_{15} & S_{26} & S_{55} + S_{66} \end{bmatrix} \} \tag{26}$$

Since $\int_{-1}^{+1}\int_{-1}^{+1} p_\xi \mathbb{N}_{o,\xi}^T \mathbb{N}_{o,\xi} d\xi d\eta$, $\int_{-1}^{+1}\int_{-1}^{+1} p_\eta \mathbb{N}_{o,\eta}^T \mathbb{N}_{o,\eta} d\xi d\eta$ etc. in $\mathbb{G}_h$ are element-independent, they can be pre-computed. Consequently, the stabilization vectors which are the matrix rows in $\mathbb{G}_h$ can be formed by multiplying the transpose of the vector $\underline{\mathbf{X}} + \underline{\mathbf{U}}$ with some element-independent precomputed matrices. The stabilization matrix $\mathbb{G}_h^T \mathbb{H}_h^{-1} \mathbb{G}_h$ and thus the entire element implementation does not require the use of higher order integration rule. Furthermore, the EAS modes which are not shared by the adjacent elements can be condensed before assemblage.

6. BENCHMARK PROBLEMS

The linear version of present element for homogeneous materials has been examined by a number of commonly employed benchmark tests including patch tests, circular plate, square plate, hemispherical shell, pre-twisted cantilever and cylindrical shells. In these problems, the element shows no sign of shear, membrane and thickness lockings. Moreover, its predictions are exceptionally close to that reported by a previous hybrid-stress solid-shell element [20] and thus will not be repeated here.

In this section, six large displacement problems will be presented and most of them involve nonlinear hyperelastic materials. The full Newton-Raphson iteration method is employed and the convergence criterion is taken to be :

$$\frac{\text{Euclidean norms of } \Delta\underline{\mathbf{U}}}{\text{Euclidean norms of } \underline{\mathbf{U}}+\Delta\underline{\mathbf{U}}} < 0.1\%$$

All problems are modeled by one layer of elements in the thickness direction. Both two- and three-point quadratures have been attempted for the thickness integration. Since they yield very close results, the former will be adopted for higher computational efficiency.

6.1 Hemispherical Shell subjected to Alternating Radial Point Forces

A hemisphere with an 18^{O} circular cutout at its pole is loaded by a pair of radially inward and a pair of radially outward point forces. The material is linear isotropic with $E = 6.825\times10^{7}$ and $\nu = 0.3$. In other words, the strain energy potential is :

$$A = \frac{\Lambda}{2}(\varepsilon_{ii})^2 + \mu\,\varepsilon_{ij}\varepsilon_{ji} \tag{27}$$

where

$$\mu = \frac{E}{2(1+\nu)} \quad \text{and} \quad \Lambda = \frac{\nu E}{(1+\nu)(1-2\nu)} \quad \text{are the Lame's constants.}$$

Owing to symmetry, a quarter of the shell is considered and modeled by an 8×8 mesh as shown in Figure 2. The radial deflections at the points A and B obtained by *NSTEP* = 1, 2, 4 and 10 as well as the total number of iterations involved are listed in Table 1. The load-deflection curves traced by using 10 load steps are plotted in Figure 3 whereas the deformed shell under the maximum load is portrayed in Figure 4. The present element and Park, Cho & Lee's eighteen-node plane-stress solid-shell element [19] are close in predictions and convergent characteristic. The results are insensitive to the number of load increments.

Table 1. Converged deflections of the hemispherical shell in Figure 9 at $P = 400$.

	NSTEP	1	5	10
present	U_A (in)	3.9932	3.9940	3.9979
	$-V_B$ (in)	7.9441	7.9452	7.9516
	total number of iterations	9	22	38
Park & Lee [6]	U_A (in)	4.0205	4.0209	4.0209
	$-V_B$ (in)	8.0160	8.0169	8.0169
	total number of iterations	8	23	35

6.2 Post-Buckling Analysis of Cylindrical Roof subjected to Central Point Load

Figure 5 shows a cylinder roof subjected to a central point load P. The straight edges are hinged and the curved edges are free. The material is linear isotropic with E = 3.10275 and ν = 0.3. The two thickness being considered are 12.7 and 6.35. Owing to symmetry, one quarter of the shell is considered and modeled by 2×2 elements. The hinged supporting condition is implemented by prescribing all the average translations of the nodes at the two director end-points to zero. Owing to the structural instability, the problem is solved by using the arc-length solver. Figure 6 plots the applied load against the central deflection. The curves for the thicker and thinner roofs closely follow that reported by Crisfield [30] and Chang & Sawamiphakdi [31], respectively.

6.3 Tapered Plane Strain Panel

Figure 7 shows the undeformed and the deformed shapes of a unit-thickness tapered plane-strain panel whose left end is fully clamped. A uniformly distributed upward shear force of total magnitude P is applied to the other end. The maximum P is 100 units. This finite deformation elasticity problem is often considered for testing the element's behavior under the quasi-incompressible condition. In the present example, the plane strain condition is imposed by restraining all the out-of-plane nodal displacements. The compressible Neo-Hookean material model with the following form of strain energy density potential is employed:

$$A = \frac{\mu}{2}\left(b_{ii} - 3\right) - \mu \ln(F) + \frac{\Lambda}{4}(F^2 - 1 - 2\ln F) \tag{28}$$

where

$b_{ij} = F_{ki}F_{kj}$ is the Right Cauchy-Green deformation tensor,

$F_{ij} = \partial(X_i + U_i)/\partial X_j$ is the deformation gradient and $F = \det(F_{ij})$.

To mimic the quasi-incompressible response, Λ should be taken to be much larger than μ. The material properties are Λ = 400890 and μ = 80.19, so that quasi-incompressible response is effectively obtained. A convergence study for the finite element meshes is given in Figure 8. The present element and the four-node plane element of Simo & Armero [1] and the eight-node solid-shell element of Betsch, Gruttmann & Stein [16] all converge to the same solution.

6.4 Clamped Circular Plate under Distributed Transverse Load

A fully clamped circular plate made of the same Neo-Hookean material as in the last example is subjected to uniformly distributed transverse load of intensity q unit force per unit area. Owing to the symmetry of load and structure, only one quarter of the plate is considered and modelled by 48

elements as shown in Figure 9. Radius and thickness of the plate are 10 and 1, respectively. The maximum q is 2.004845. Figure 10 shows the curve of the applied load q versus the central deflection which is in excellent agreement with the exact solution given by Schieck, Pietraszkiewicz & Stumpf [4]. Figure 11 portrays the deformed mesh at the maximum load q.

6.5 Cantilever Plate

Figure 12 depicts the deformed and undeformed shapes of a rectangular cantilever plate subjected to a uniformly distributed load at the free end. The plate is of unit thickness. The material parameters are $\Lambda = 9998$ and $\mu = 2$. The maximum load q is set to 0.01 unit force per unit length. Owing to symmetry, half of the plate is considered and modeled by 1×4 and 3×10 elements. The same problem was also analyzed by using 20×5×1 and 40×10×2 MSC.Marc eight-node brick elements of element designation 117 [33]. Further mesh refinement does not yield any graphically distinguishable results. The strain energy potential for the incompressible neo-Hookean material model available in MSc.MARC is :

$$A = \frac{\mu}{2}\left(b_{ii} - 3\right) \tag{29}$$

Figure 13 plots load q against the deflection at point A. The predictions by the 40×10×2 MSC.Marc eight-node brick elements and the 1×4 present elements are very close. Meanwhile, the predictions by the present element using the 1×4 and 3×10 meshes are graphically indistinguishable.

6.6 Hyperelastic Cylindrical Shells subjected to a Line Force

The open-ended cylinder depicted in Figure 14 rests on a rigid line support and is subjected to a uniform line force whose total magnitude is P. The compressible Neo-Hookean material model with the following form of strain energy density potential is employed:

$$A = \frac{\Lambda}{2}(\ln F)^2 - \mu \ln(F) + \frac{\mu}{2}(b_{ii} - 3) \tag{30}$$

in which F and b_{ij} have been defined in (28). Moreover, $\Lambda = 24{,}000$ and $\mu = 6{,}000$. Owing to symmetry, one quarter of the cylinder is analyzed and modeled by a uniform 8×4 mesh. The mean diameter of the shell is 18 and thickness h = 2 and 0.2 cm are considered. The cylinder behaves similar to a ring and the deflection under the line force is fairly uniform. Figure 15 plots the load against the deflection at A, W_A, of the thick cylinder. The result of Bücher, Ramm & Roehl [15]

was predicted by using 16×6 eight-node seven-parameter shell elements and the result of Hauptmann, Schweizerhof & Doll [17] was obtained by using 16×12 eight-node solid-shell elements. Prediction of the present element is between that of Bücher, Ramm & Roehl and Hauptmann, Schweizerhof & Doll. Figure 16 shows the deformed cylinders.

Table 2: Convergence studies for the hyperelastic cylinder problem in Figure 14.

number of elements in circumferential direction	$-W_A$ of the thin shell at P = 34		$-W_A$ of the thick shell at P = 30,000	
	present	reference 15	present	reference 15
4	13.3	10.0	14.6	13.4
8	15.4	14.3	16.2	15.9
16	15.6	15.6	16.4	16.4
converged result	15.6		16.4	

7. CLOSURE

A hybrid-strain stabilization procedure is developed for an eighteen-node solid-shell element for large deformation analysis of hyperelastic shell structures. To overcome the thickness locking of the element, the enhanced assumed thickness strain modes are incorporated. Compared to the pertinent URI element, the present element possesses a low-cost stabilization matrix which can be computed without using numerical integration loop. The stabilization matrix is of prime importance as the global tangential stiffness matrices resulting from the URI elements often become singular after a few iterations. The proposed element has been examined with a number of commonly employed benchmark tests. Its performance is promising and the predictions are in good agreement with other published works.

Acknowledgment – The financial support of the *Research Grant Council of Hong Kong* (project number : HKU7101/99E) is gratefully acknowledged.

REFERENCES

1. J.C.Simo, F.Armero. Geometrically non-linear enhanced strain mixed methods and the method of incompatible modes. *Inter.J.Numer.Methods Engrg*., **33**, 1413-1449 (1992)
2. J.C.Simo, R.L.Taylor. Quasi-incompressible finite elasticity in principal stretches continuum basis and numerical algorithms., *Comput.Methods Appl.Mech.Engrg.*, **85**, 273-310 (1991)
3. F.Gruttmann, R.L.Taylor. Theory and finite element formulation of rubberlike membrane shells using principal stretches. .*Inter.J.Numer.Methods Engrg*., **35**, 1111-1126 (1992)
4. B.Schieck, W.Pietraszkiewicz, H.Stumpf. Theory and numerical analysis of shells undergoing large elastic strains. *Int.J.Solids & Struct.*, **29**, 689-709 (1992)
5. C.Miehe, Aspects of the formulation and finite element implementation of large strain isotropic elasticity. *Inter.J.Numer.Methods Engrg*., **37**, 1981-2004 (1994)
6. P.Wrigger, U.Hueck. A formulation of the QS6 element for large elastic deformations. *Inter.J.Numer. Methods Engrg*., **39**, 1437-1454 (1996)
7. S.Reese, P.Wriggers. A finite element method for stability problems in finite elasticity. *Inter.J.Numer. Methods Engrg*., **38**, 1171-1200 (1995)
8. J.C.Nagtegnall, D.D.Fox. Using assumed enhanced strain elements for large compressible deformation. *Int.J.Solids & Structures*., **33**, 3151-3159 (1996)
9. S.Reese, M.Küssner, B.D.Reddy. A new stabilization technique for finite elements in non –linear elasticity. *Inter.J.Numer.Methods Engrg*., **44**, 1617-1652 (1999)
10. S.Reese, P.Wriggers, B.D.Reddy. A new locking-free brick element technique for large deformation problems in elasticity. *Computers & Structures*, **75**, 291-304 (2000)
11. F.Gharzeddine, A.Ibrahimbegovic. Incompatible mode method for finite deformation quasi-incompressible elasticity. *Comput. Mech*, **24**, 419-425 (2000)
12. Y.Basar, M.Itskov. Finite element formulation of the Ogden material model with application to rubber-like shells. *Inter.J.Numer.Methods Engrg*., **42**, 1279-1305 (1998)
13. Y.Basar, Y.Ding. Shear deformation models for large strain shell analysis. *Int.J.Solids & Structures*., **34**, 1687-1708 (1997)
14. Y.Basar, Y.Ding. Finite element analysis of hyperelastic thin shell with large strains. *Comput.Mech*, **18**, 200-214, (1996)
15. N.Bücher, E.Ramm, D.Roehl. Three-dimensional extension of non-linear shell formulation based on the enhanced assumed strain concept. *Inter.J.Numer.Methods Engrg*., **37**, 2251-2568 (1994)
16. P.Betsch, F.Gruttmann, E.Stein. A 4-node finite shell element for the implementation of general hyperelastic 3D-elasticity at finite strains. *Comput.Methods Appl.Mech.Engrg.*, **130**, 57 –79 (1996)
17. R.Hauptmann, K.Schweizerhof, S.Doll. Extension of the 'solid-shell' concept for application to large elastic and large elastoplastic deformations. *Inter.J.Numer.Methods Engrg*., **49**, 1121 –1141(2000)
18. Y.H.Kim, S.W.Lee. A solid element formulation for large deflection analysis of composite shell structures. *Computers & Structures*, **30**, 269-274 (1988)
19. H.C.Park, C.Cho, S.W.Lee. An efficient assumed strain element model with 6 dof per node for geometrically nonlinear shells. *Inter.J.Numer.Methods Engrg*., **38**, 4101- 4122 (1995)
20. K.Y.Sze, S.Yi, M.H.Tay. An explicit hybrid-stabilized eighteen-node solid element for thin shell analysis. *Inter.J.Numer.Methods Engrg*., **40**, 1839- 1856 (1997)
21. K.Y.Sze**,** S.-J.Zheng. A stabilized hybrid-stress solid element for geometrically nonlinear homogeneous and laminated shell Analyses. *Comput.Methods Appl.Mech.Engrg.*, **191**, 1945-1966 (2002)
22. K.Y.Sze, W.K.Chan, T.H.H.Pian. An eight-node hybrid-stress solid-shell element for geometric nonlinear analysis of elastic shells. *Inter.J.Numer.Methods Engrg*., **55**, 26 journal pages (2002)
23. K.Y.Sze, A.Ghali, Hybrid hexahedral element for solids, plates, shells and beams by selective scaling. *Inter. J.Numer.Methods Engrg.*, **36**, 1519-1540 (1993)
24. K.Y.Sze, S.Yi, M.H.Tay. An explicit hybrid-stabilized eighteen-node solid element for thin shell analysis. *Inter.J.Numer.Methods Engrg*., **40**, 1839-1856 (1997)

25. K.Y.Sze, L.Q.Yao. A hybrid-stress ANS solid-shell element and its generalization for smart structure modelling - part I : solid-shell element formulation, part II : smart structure modeling. *Inter.J.Numer. Methods Engrg*., **48**, 545-582 (2000)
26. K.Y.Sze, S.H.Lo, L.Q.Yao. Hybrid-stress solid elements for shell structures based upon a modified variational functional. *Inter.J.Numer.Methods Engrg*., **53**, 2617-2642 (2002)
27. J.C.Simo, M.S.Rifai, D.D.Fox. On a stress resultant geometrically exact shell model – part IV : variable thickness shells with through-the-thickness stretching. *Computer Methods Appl.Mech. Engrg.*, **81**, 91-126 (1990)
28. K.Y.Sze, "Admissible matrix formulation : from orthogonal approach to explicit hybrid-stabilization", *Finite Elements in Analysis & Design*, **24**, 1-30 (1996)
29. R.L.Taylor, J.C.Simo, O.C.Zienkiewicz, C.H.Chan, "The patch test - a condition for assessing fem convergence", *Inter.J.Numer.Methods Engrg.*, **22**, 39-62 (1986)
30. M.A.Crisfield. Non-linear Finite Element Analysis of Solids & Structures. Volume 2: Advanced Topics. John Wiley & Sons, 1997
31. T.Y.Chang & K.Sawamiphakdi, Large deformation analysis of laminated shells by finite element method, *Comp. & Struct*., **13**, 331-340 (1981)
32. J.C.Simo, F.Armero & R.L.Taylor. Improved versions of assumed enhanced-strain tri-linear elements for 3D finite deformation problems. *Comput.Methods Appl.Mech.Engrg.*, **110**, 359 –386 (1993)
33. *MSC.Marc 2000 User Manual*, MSC.Software Corporation, LA, USA, 2000.

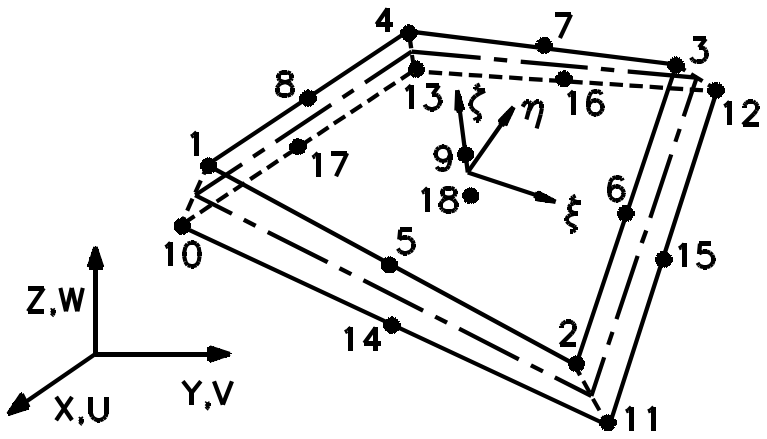

Figure 1. An eighteen-node solid-shell element.

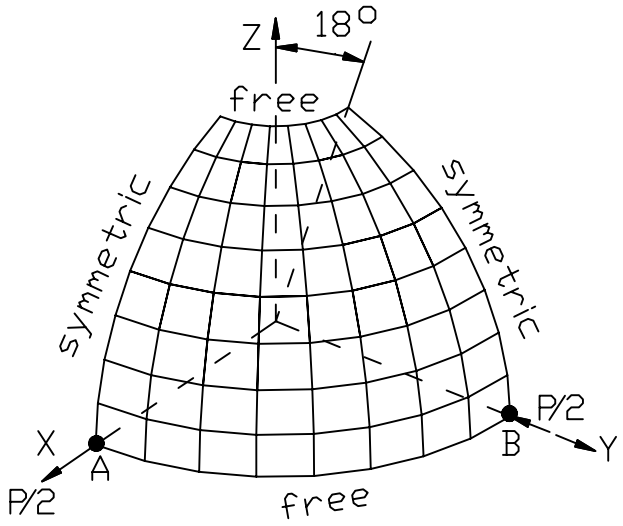

Figure 2. The 8x8 mesh employed to model a quarter of the hemispherical shell under alternating radial point forces. $R = 10$, $h = 0.04$ and $P_{max} = 400$.

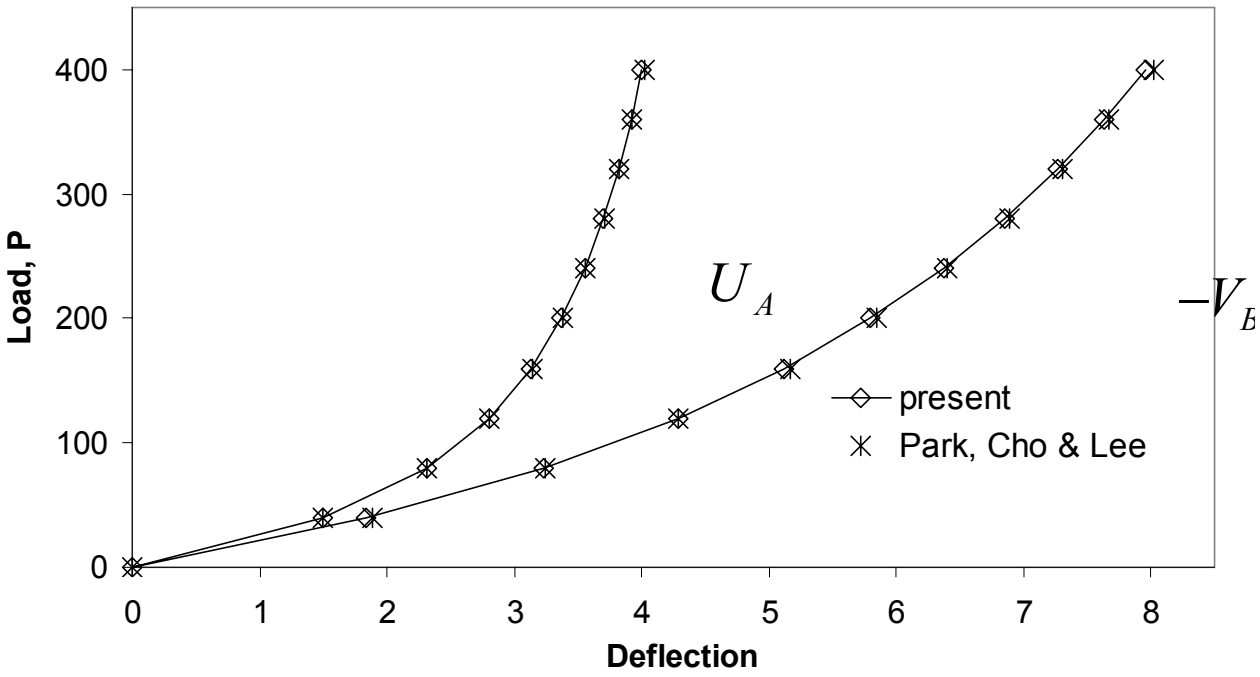

Figure 3. The load-deflection curves at points A and B, see Figure 2.

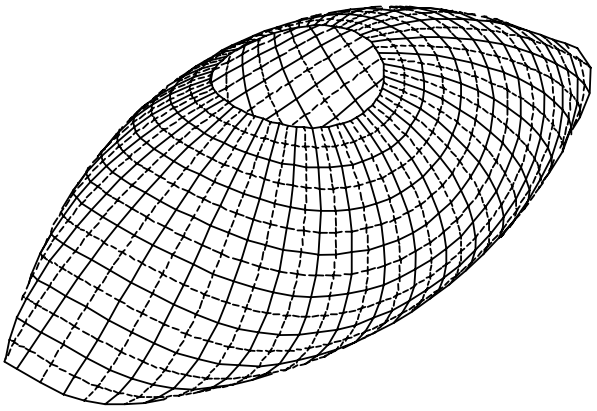

Figure 4. The deformed hemisphere of Figure 2 at $P = 400$.

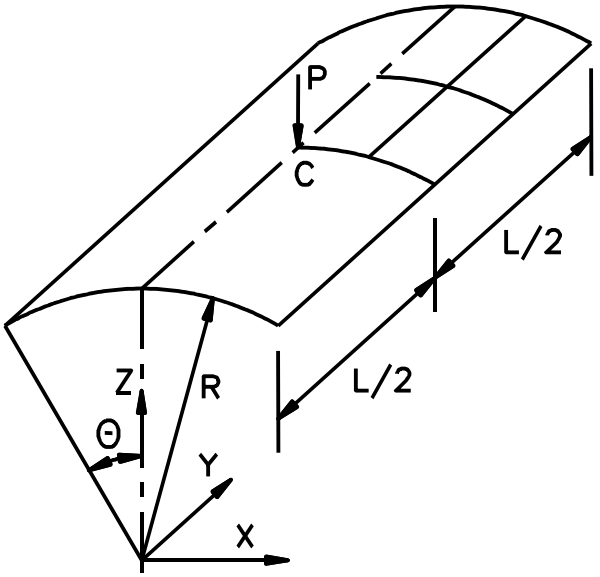

Figure 5. A cylindrical roof subjected to a central point load *P*. Straight edges are hinged, curved edges are free, $R = 2540$, $L = 508$, $\theta = 0.1$ radians, $h = 12.7$ or 6.35.

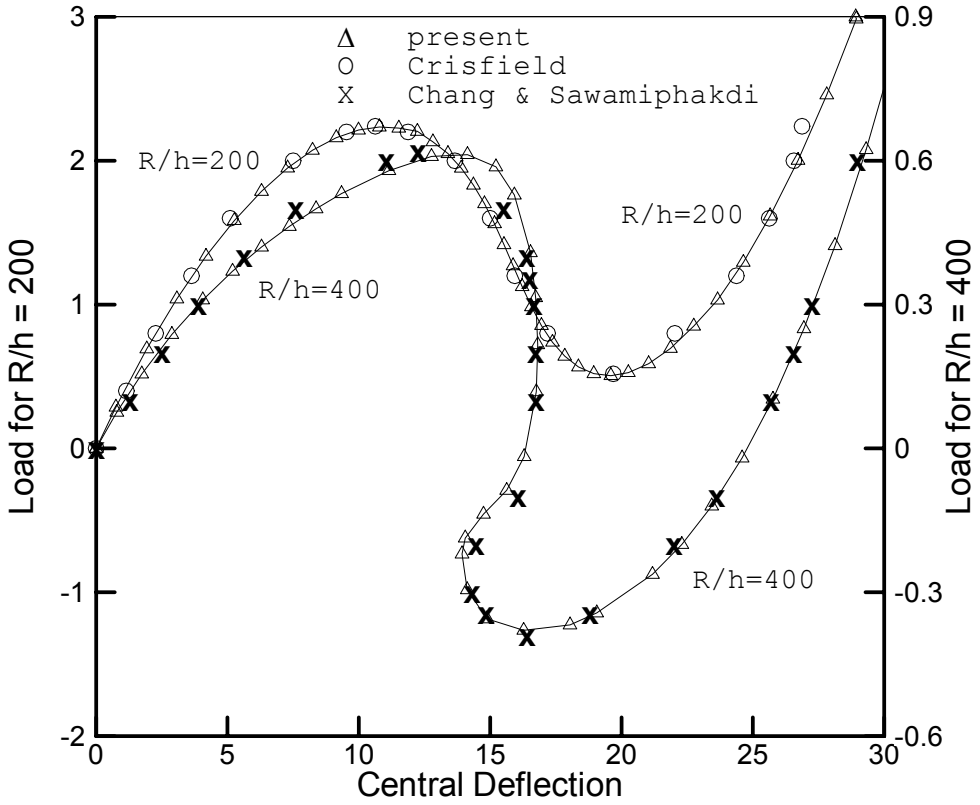

Figure 6. Post-buckling behaviour of the cylindrical roof of Figure 5.

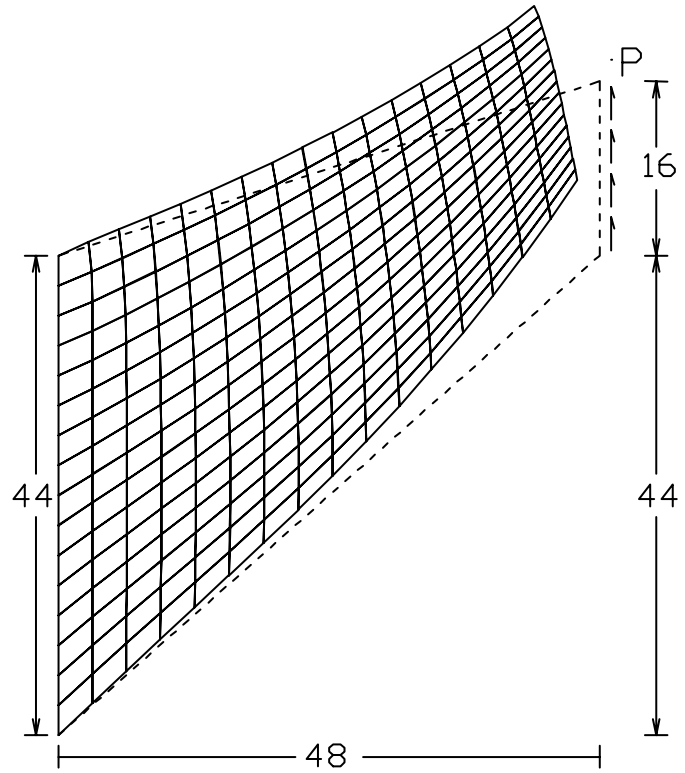

Figure 7. The undeformed unit-thickness plane-strain panel and its deformed mesh (16×16 elements) at P = 100 unit force.

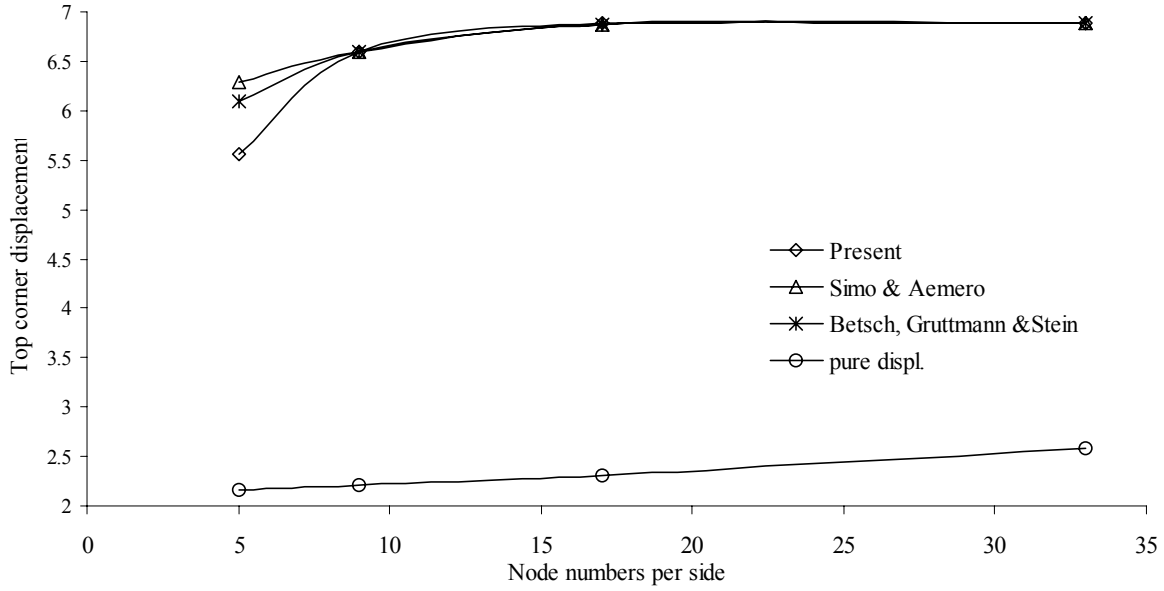

Figure 8. Convergence of the top corner displacement in the plane strain panel problem, see Figure 7.

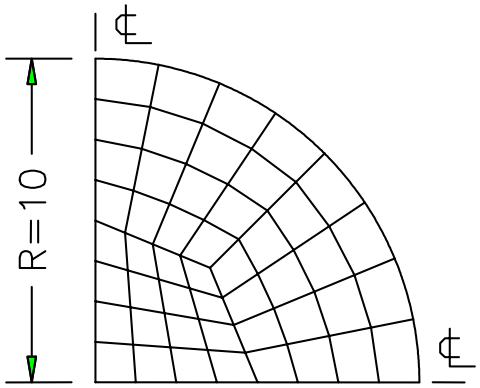

Figure 9. A quadrant of the clamped circular plate modelled by 48 elements.

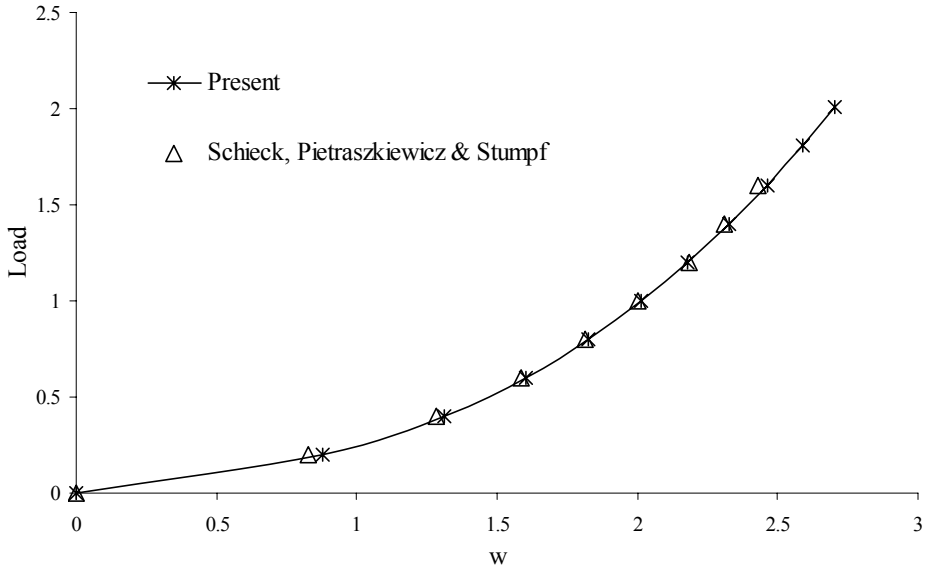

Figure 10. Load against center deflection curve for the clamped circular plate of Figure 9.

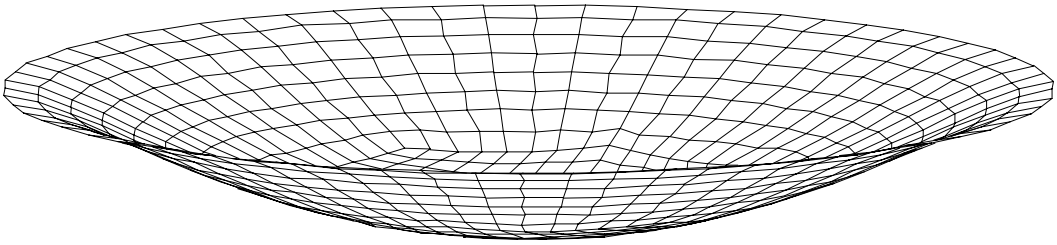

Figure 11. The deformed circular plate of Figure 9 at q = 2.004845.

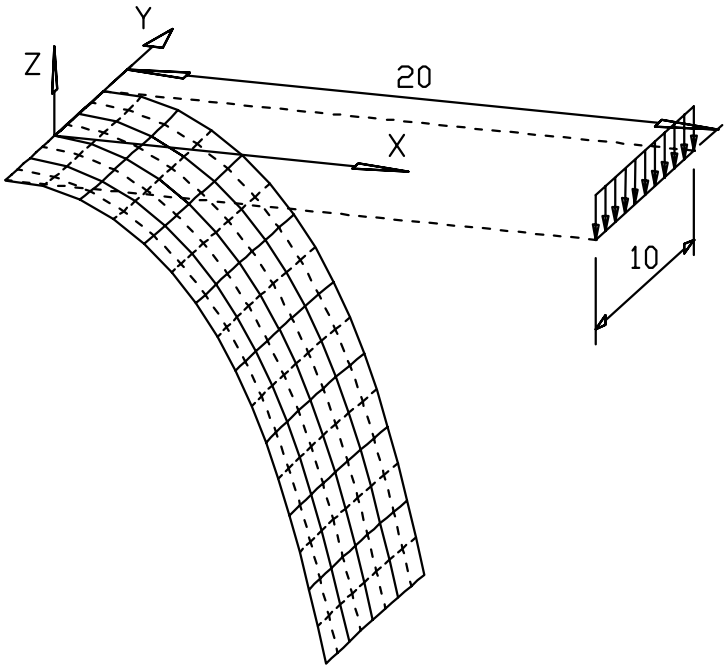

Figure 12. The deformed (8×4) mesh for the cantilever plate subjected to end line force of unit magnitude per unit length. The plate thickness is 1 unit.

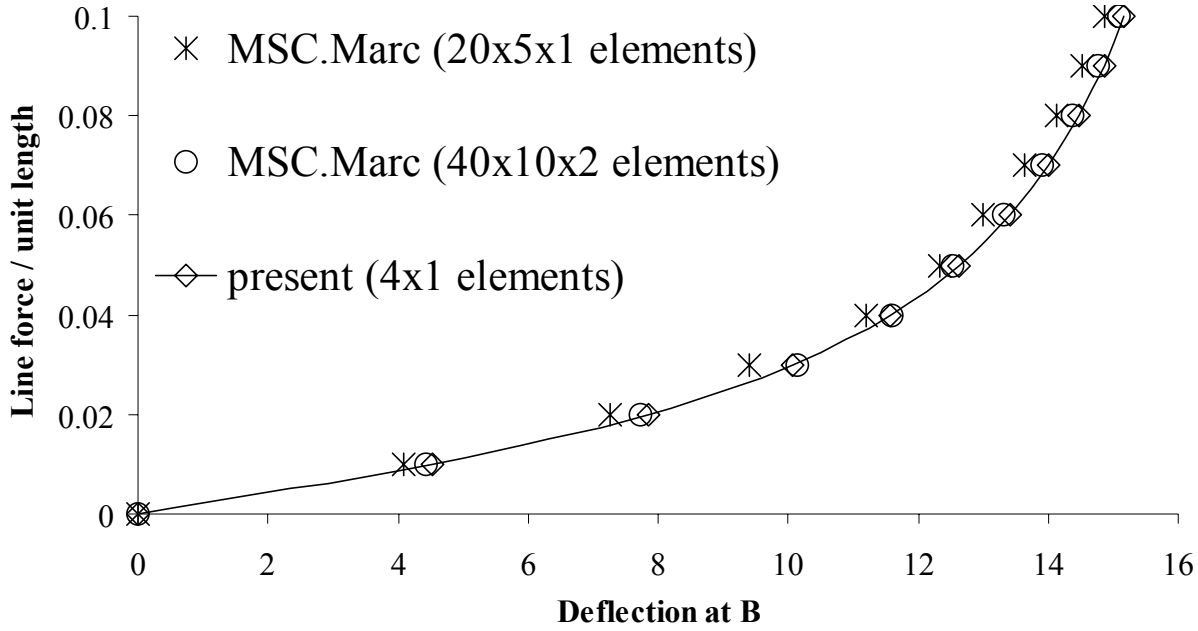

Figure 13. The load-deflection curve for the cantilever plate problem of Figure 12.

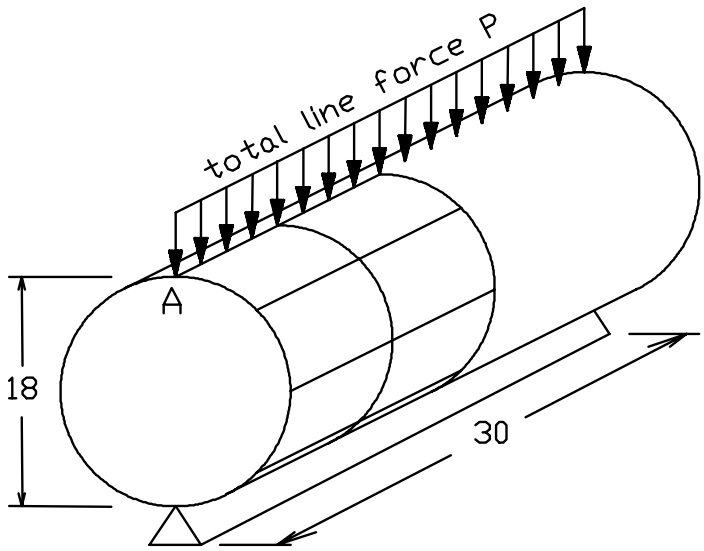

Figure 14. One quarter of the open-ended cylindrical shell problem modeled by the uniform 4×2 mesh. The thickness under consideration are $h = 0.2$ and $h = 2$.

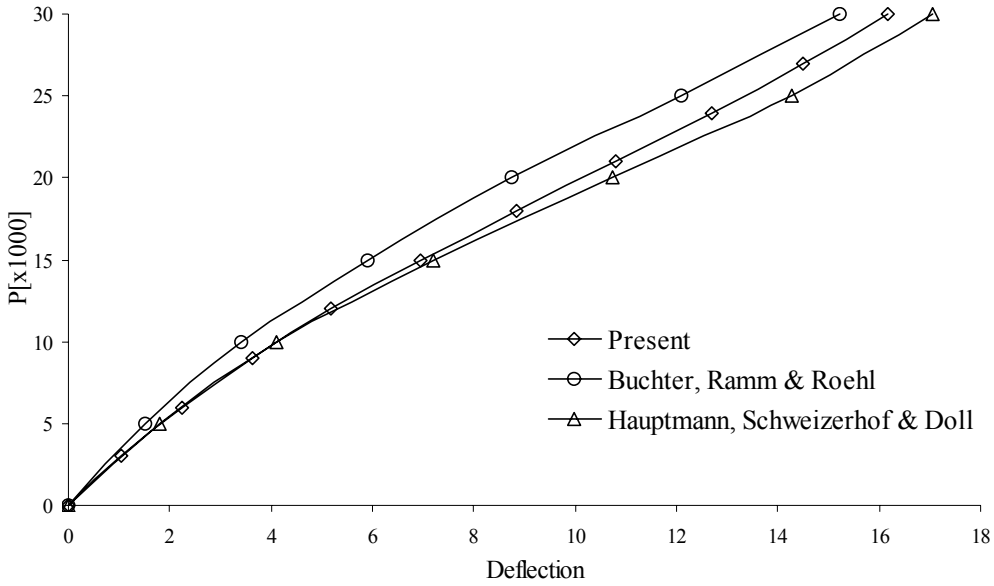

Figure 15. Load against radial deflection curve for the thick cylindrical problem of Figure 14.

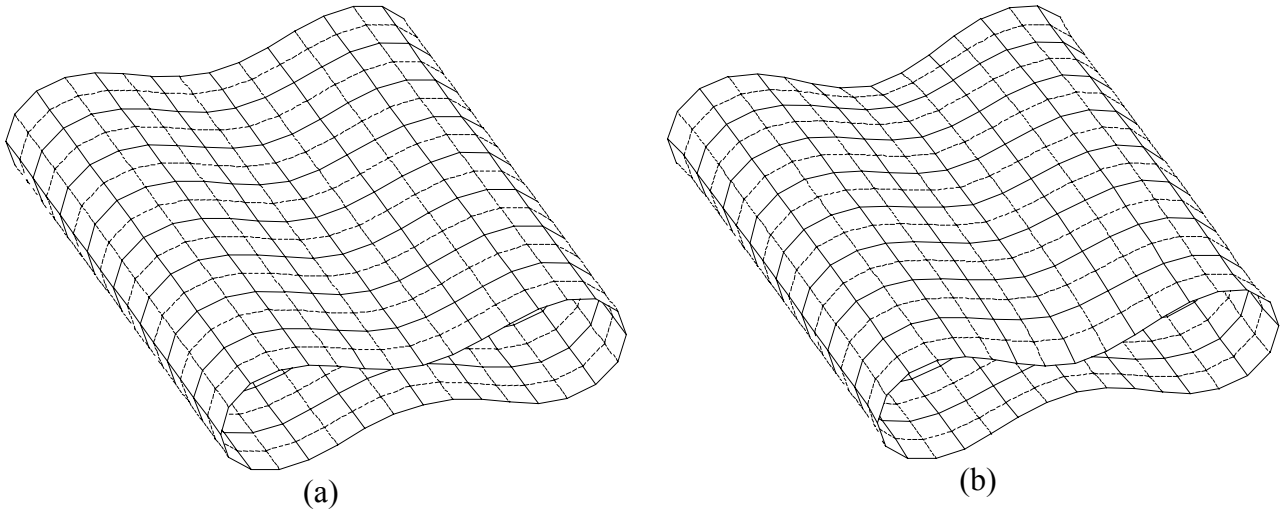

Figure 16. (a) The deformed thin cylinder at P = 34 and (b) the deformed thick cylinder at P = 30,000, see Figure 14.